

Supporting Information

Stacking as a Key Property for Creating Nanoparticles with Tunable Shape: The Case of Squalenoyl-Doxorubicin

Julie Mougin[†], Semen O. Yesylevskyy^{‡,¶}, Claudie Bourgaux[†], David Chapron[†], Jean-Philippe Michel[†], Franco Dosio[§], Barbara Stella[§], Christophe Ramseyer[¶], Patrick Couvreur^{,†}*

[†]Institut Galien Paris-Sud UMR CNRS 8612, Faculty of Pharmacy, Univ. Paris-Sud, Université Paris-Saclay, 92290 Châtenay-Malabry, France

[‡]Department of Physics of Biological Systems, Institute of Physics of the National Academy of Sciences of Ukraine, Prospect Nauky 46, 03028 Kyiv, Ukraine

[§]Dipartimento di Scienza e Tecnologia del Farmaco, Università degli Studi di Torino, 10125 Turin, Italy

[¶]Laboratoire Chrono Environnement UMR CNRS 6249, Université de Bourgogne Franche-Comté, 16 route de Gray, 25030 Besançon Cedex, France

*To whom correspondence should be addressed: patrick.couvreur@u-psud.fr

I. SUPPLEMENTARY FIGURES

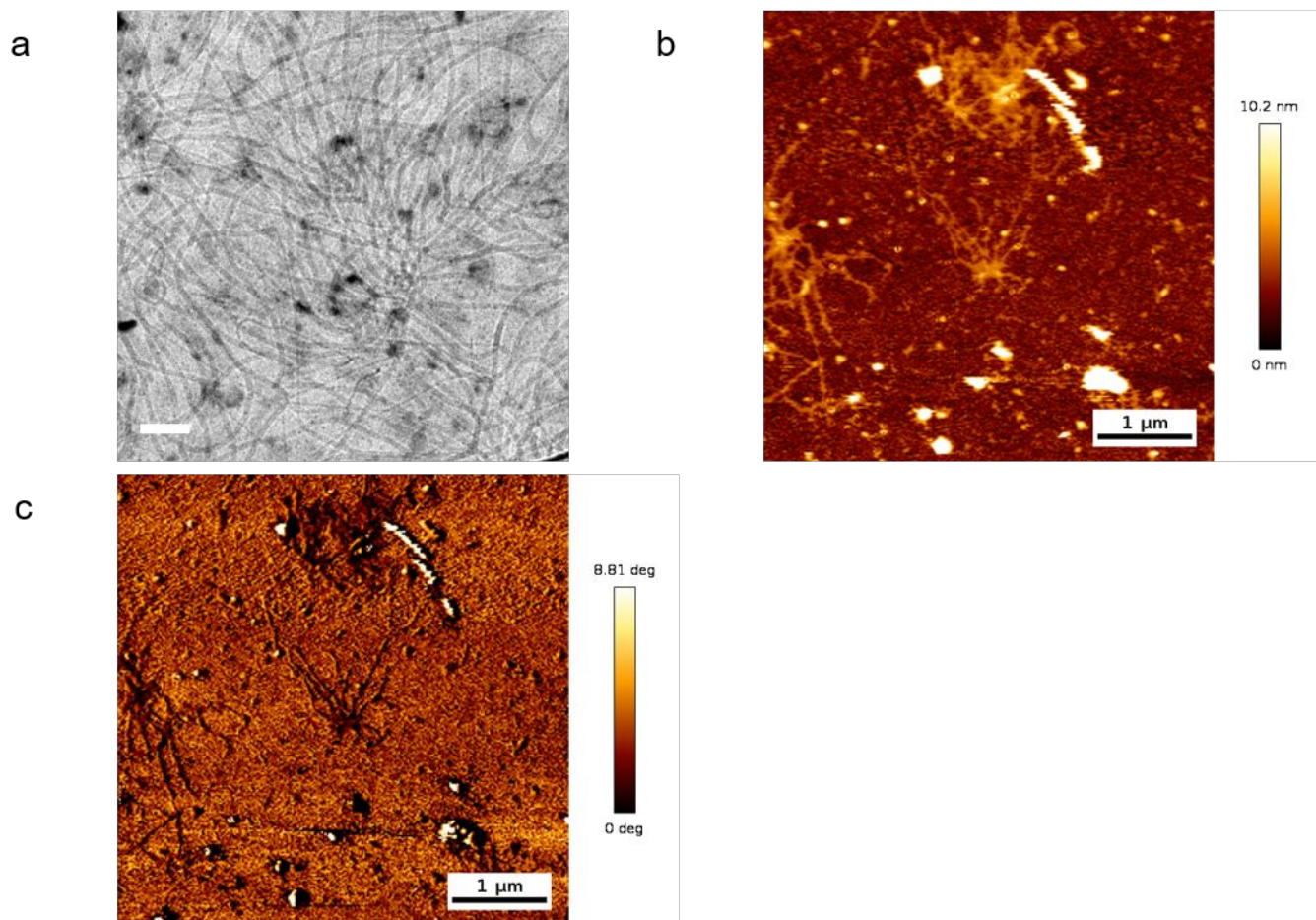


Figure S1. (a) Additional cryo-TEM micrograph of nanoparticles prepared at 4 mM in H₂O (Scale bar, 100 nm). (b), (c) AFM pictures obtained in liquid medium of SQ-Dox nanoparticles prepared at 4 mM in water and diluted to 20 μM (Scale bar, 200 nm). (b) Height image. (c) Phase image.

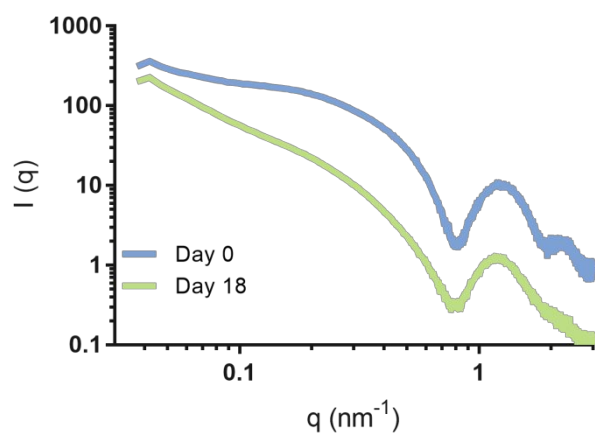


Figure S2. Ageing effect on SAXS patterns of SQ-Dox nanoparticles prepared at 4 mM. SQ-Dox long wormlike nanoparticles are detected after several days: in the low q -range ($q \leq 0.6$ nm⁻¹), $I(q)$ could be fitted with the Kholodenko model. Curves are shifted along the y-axis for clarity.

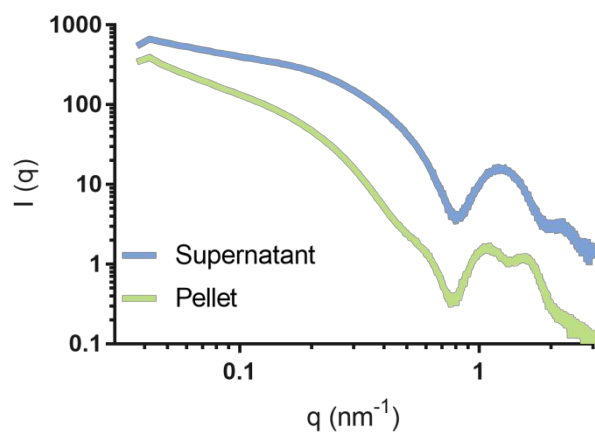


Figure S3. SAXS pattern of SQ-Dox nanoparticles prepared at 8 mM, after ultracentrifugation. The supernatant curve corresponds to short cylindrical nanoparticles (length ~ 20 nm) while the pellet curve indicates the presence of longer aggregated nanoparticles. At $q < 0.4$ nm⁻¹ curve fitting suggests that bundles of about three cylinders, with length ≥ 100 nm, are mostly formed while at $q > 0.4$ nm⁻¹, the SAXS curve is consistent with the stacking of core-shell cylinders. Curves are shifted along the y-axis for clarity.

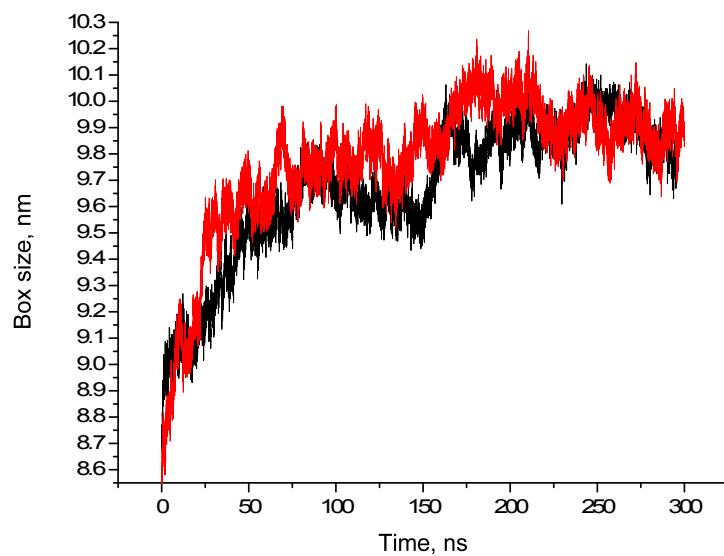


Figure S4. Evolution of the box size in the course of equilibration of SQ-Dox cylindrical nanoparticles. The equilibrium is reached after ~ 200 ns. Results of two independent simulations are shown.

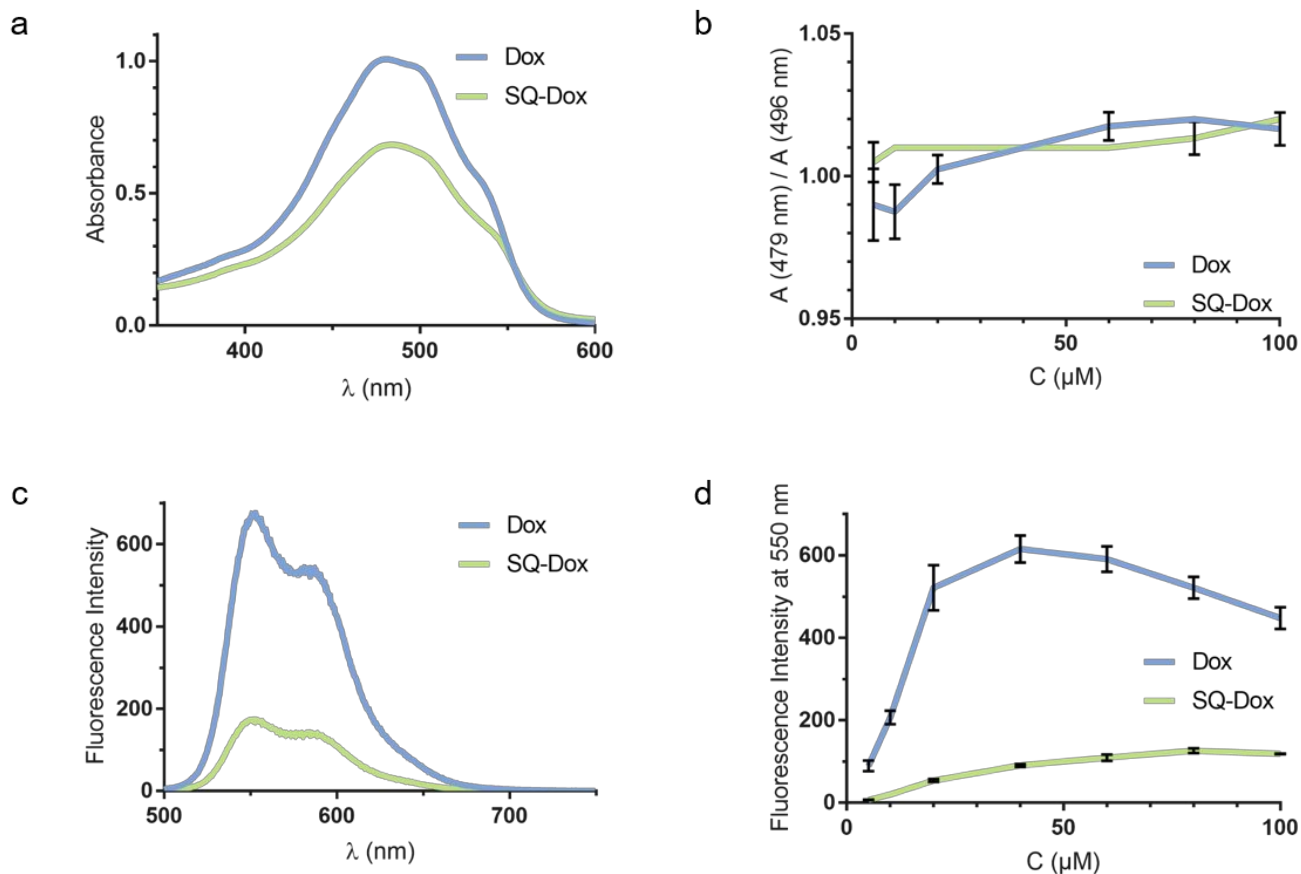


Figure S5. Dox and SQ-Dox spectroscopic properties and stacking characterization. (a) Absorbance plots of SQ-Dox nanoparticles and free Dox diluted in water at 104 μM . The Dox absorption spectrum displays three bands characteristic of the anthracycline rings in the visible region (479, 496 and 529 nm). Stacking is known to lead to a significant hypochromism in the spectral region below 540 nm and a weak hyperchromism above 540 nm.¹ This highlights the stronger stacking in SQ-Dox nanoparticles than in free Dox solutions. (b) Absorbance ratio of the 479 and 496 nm bands. The stacking occurs when the absorbance at 496 nm overcomes the absorbance at 479 nm, *i.e.*, $A(479 \text{ nm}) / A(496 \text{ nm}) > 1$. (c) Fluorescence spectra of SQ-Dox nanoparticles and Dox diluted in water at 52 μM after excitation at 480 nm. The fluorescence of Dox arises from the monomers and is quenched when Dox forms dimers (above $\sim 20 \mu\text{M}$ for free Dox). (d) Fluorescence intensity at 550 nm after excitation at 480 nm. The enhanced stacking of the anthracycline rings in SQ-Dox nanoparticles is demonstrated by the much lower fluorescence intensity of SQ-Dox compared to free Dox at the same molar concentration. (Data presented as mean \pm S. D.)

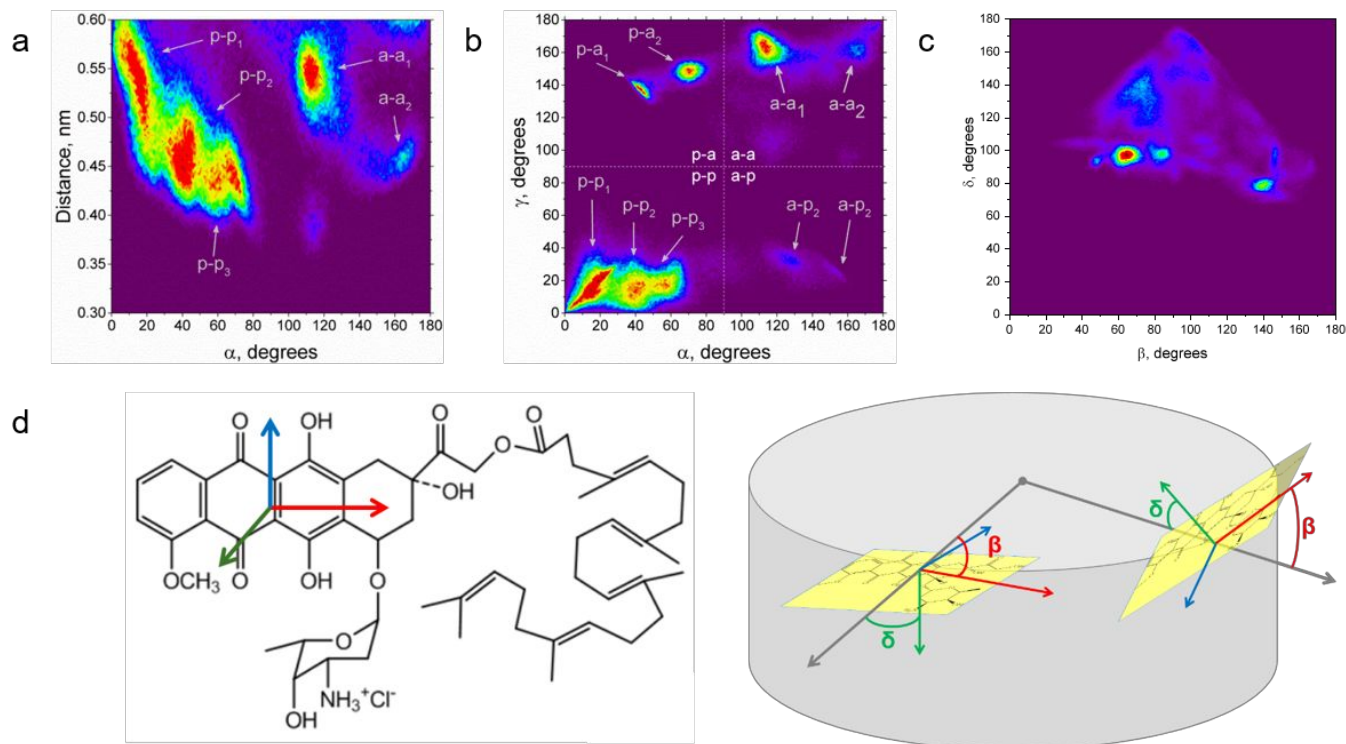


Figure S6. Properties of stacked pairs of rings and their abundances in cylindrical nanoparticles. Color shows probability of finding particular combination of parameters for each type of stacking pairs (purple correspond to zero, red is the maximum). Labels with arrows indicate subpopulations discussed in the text. The codes of aggregates correspond to Figure 2. (a) The distance-angle maps where d is the distance between the centers of masses of the rings in a stacked pair and α is the angle between long axes of the rings. (b) The angle-angle maps where α and γ are the angles between long axes and normals to the rings with the axis of cylinder. Dashed lines separate the quadrants corresponding to different types of stacked aggregates, which are shown near the crossing of these lines. (c) The orientation maps of Dox rings where β is the angle between the long axis of the ring and the radius of cylinder at the point of its center of masses. δ is the same for the normal to the ring. (d) Scheme of Dox axes and angles with radius of cylinders. Long axis is red, short axis is blue, normal axis (perpendicular to the figure) is green.

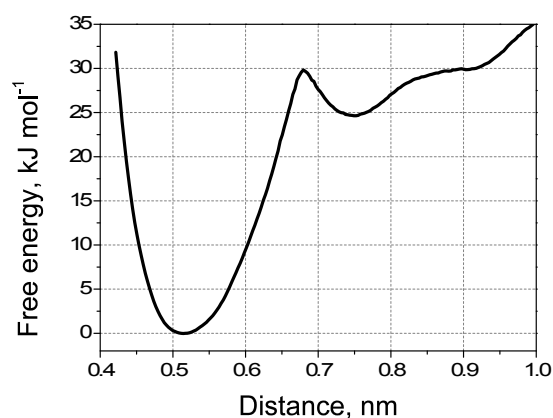


Figure S7. The potential of mean force of disrupting lone p-p₁ stacking pair in cylindrical nanoparticles. The minimum corresponds to the most favorable distance between Dox stacking pairs of type p-p₁. The optimal stacking distance is ~ 0.51 nm and the free energy rises rapidly with the increase in the distance. There is a metastable state at the distance of ~ 0.74 nm corresponding to two adjacent Dox moieties interacting by means of unspecific interactions. Further increase in the distance starts to drive two molecules away from the same coordination shell.

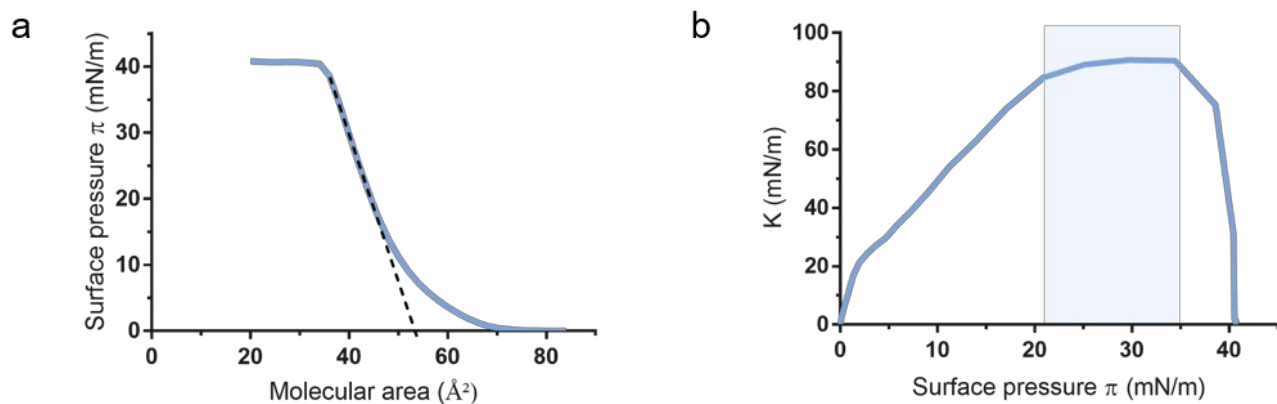


Figure S8. SQ-Dox monolayer properties. (a) Surface pressure-molecular area compression isotherm. The mean molecular area is deduced from the intersection of the tangent to the curve (dashed line) with the X axis. (b) Compressibility modulus $K = C_s^{-1}$ as a function of surface pressure. The blue domain highlights the wide pressure range corresponding to the maximum monolayer compressibility modulus, which suggests possible molecular reorganization within the monolayer.

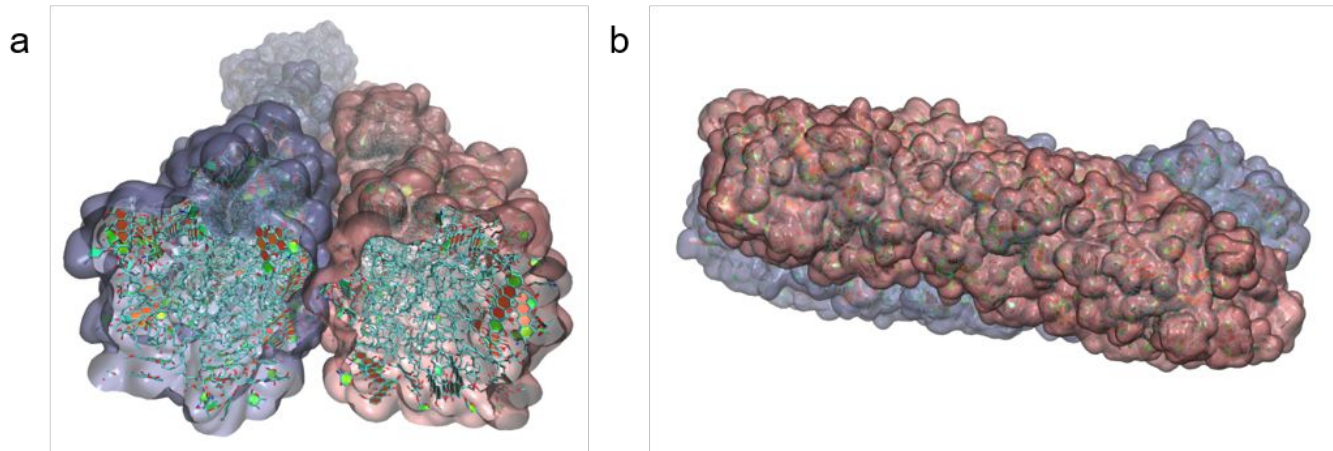


Figure S9. Interacting cylindrical nanoparticles with helical twisting. (a) Front view. (b) Side view

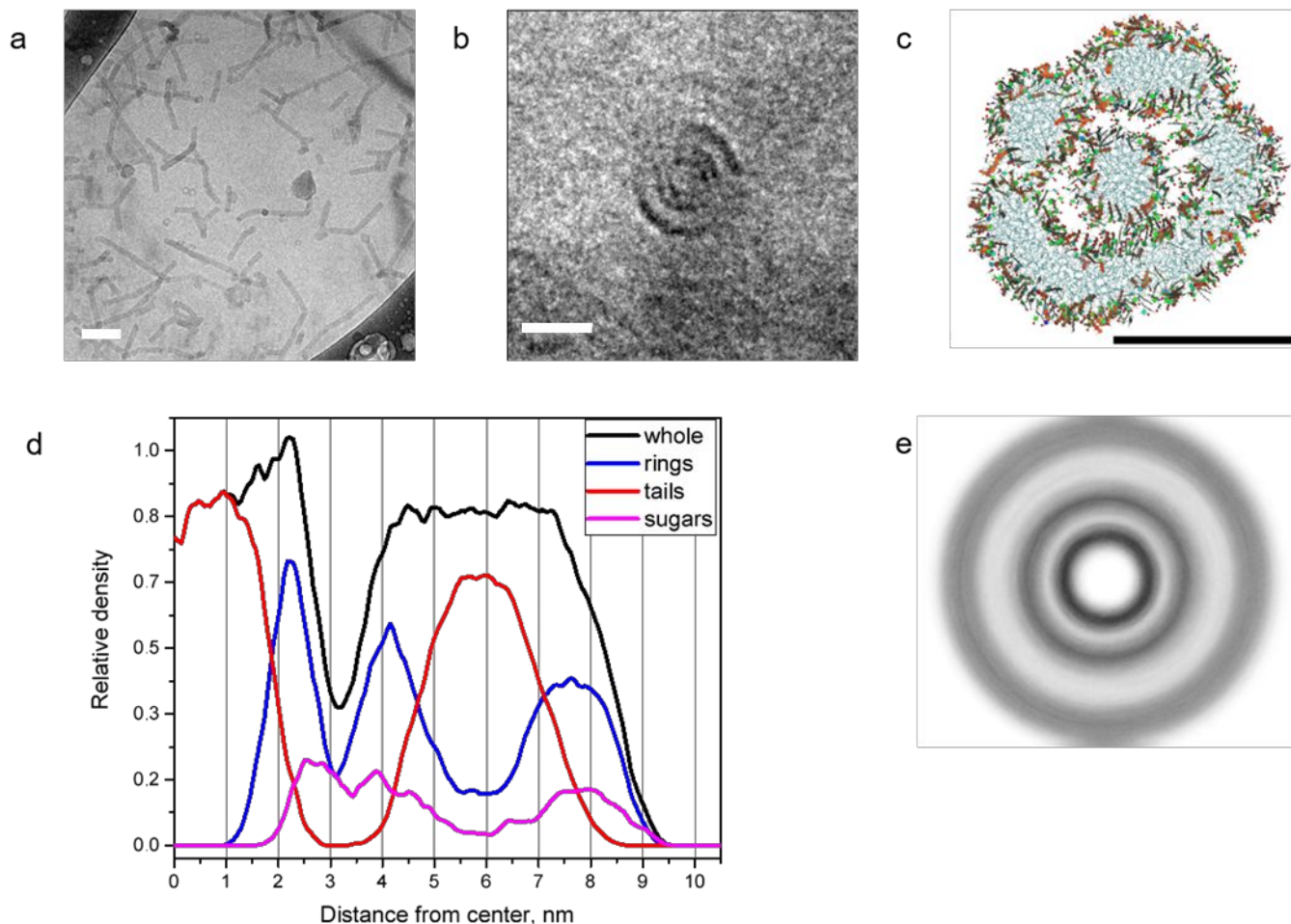


Figure S10. Structure of SQ-Dox nanotubes in the presence of divalent anions. (a) Additional cryo-TEM micrograph of SQ-Dox nanoparticles 2 mM with addition of Na_2SO_4 1 mM (molar ratio SQ-Dox: Na_2SO_4 2:1). Using divalent anion, the SQ-Dox nanoparticles are shorter, and more rigid than with monovalent anion. (Scale bar, 100 nm). (b) Cross-section of a 2 mM SQ-Dox tube with addition of 0.04 mM Na_2SO_4 (Scale bar, 10 nm). (c) Snapshot of equilibrated SQ-Dox tube. Water and ions are not shown for clarity. The colors are the same than in Figure 1. (d) Radial density distribution of the SQ chains and Dox heads in the three-layer tubes with SO_4^{2-} . (e) Density map of Dox headgroups. The black rings represent the Dox heads in the cross section of the tube computed over equilibrated part of MD trajectory and symmetrized radially around the center of the tube.

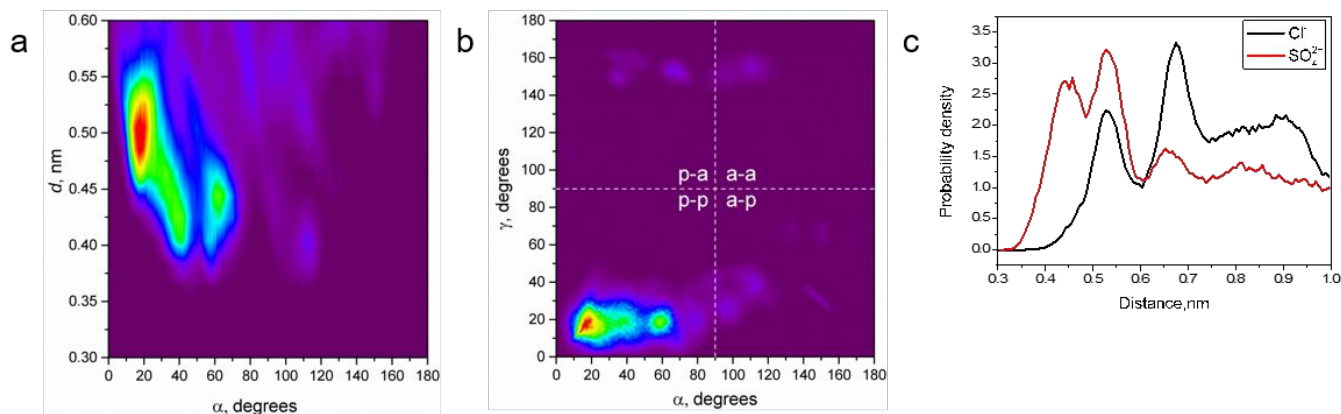


Figure S11. Properties of planar SQ-Dox bilayers. (a) Distance-angle map for the pairs of SQ-Dox rings in equilibrated bilayer. (b) Angle-angle map for the pairs of SQ-Dox rings in equilibrated bilayer. d is the distance between the centers of masses of the rings, α is the angle between long axes of the rings, γ is the angle between normals of the rings. Color shows probability of finding particular combination of parameters (purple correspond to zero, red is the maximum). Dashed lines on the panel separate the quadrants corresponding to different types of stacked aggregates, which are shown near the crossing of these lines. The codes of aggregates correspond to Figure 2. (c) Distribution of the distances between N atoms of the sugar in stacked pairs of Dox rings for Cl^- and SO_4^{2-} anions.

In simulated bilayers, different populations of stacked pairs were observed within the p-p pairs with an inclination angle of $\sim 20^\circ$ being the most abundant. Minor populations with inclination angles of $\sim 40^\circ$ and $\sim 60^\circ$ are also present. Other types of pairs (a-a, a-p, p-a) are extremely rare in equilibrated bilayers (Figure S11a,b).

II. SUPPLEMENTARY TABLE

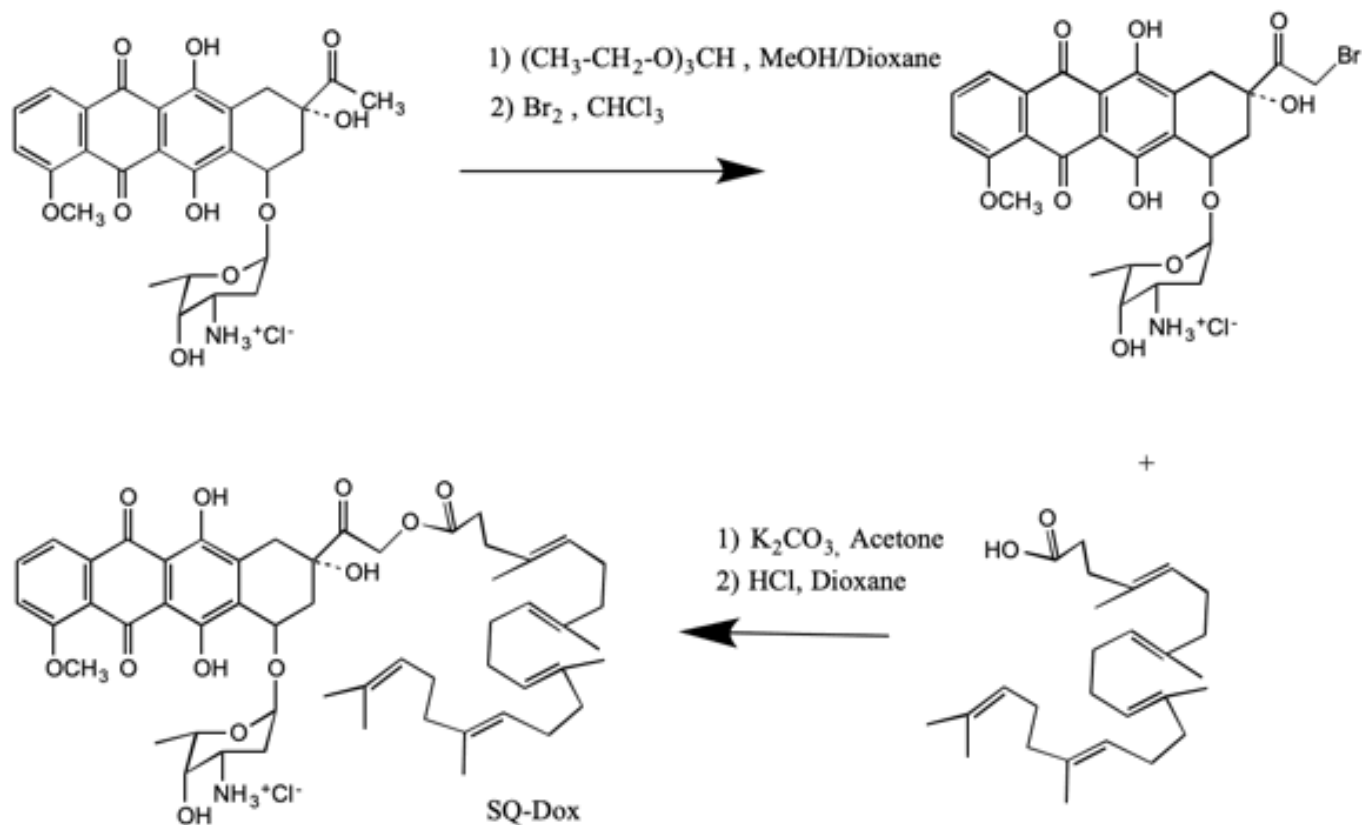
Parameter		SQ-Dox concentration				
		2 mM	4 mM	8 mM	15 mM	
λ_D (Å)	In H ₂ O	95.0	67.0	47.5	34.6	
	With added NaCl at molar ratio SQ-Dox:NaCl 1:1	54.8	38.7	27.4	/	
Volume ratio $\frac{\pi(R + \lambda_D)^2 L}{\pi R^2 L}$ <i>(R ~ 3.5 nm)</i>		In H ₂ O	13.8	8.5	5.5	3.95

Table S1: SQ-Dox nanoparticles Debye lengths

III. ADDITIONAL METHODS

Synthesis of squalenoyl-doxorubicin. Squalenoyl-doxorubicin hydrochloride (SQ-Dox) was synthesized as previously described² with some slight modifications. Trimethylorthoformate (0.20 mL, 1.83 mmol) was added to a solution of daunorubicin hydrochloride (Scheme S1, 0.20 g, 0.35 mmol) dissolved in methanol/1,4-dioxane (v/v = 1:2, 12 mL). The reaction mixture was then stirred at room temperature for 20 min. To this mixture was further added a Br₂/CHCl₃ (w/v = 1:9, 0.68 mL, 0.43 mmol) solution. After stirring for 40 min at 30 °C, the resulting solution was poured into dry ether (200 mL) and the solid residue was filtered and washed with ether (50 mL x 3). The solid was recrystallized from acetone/ether (v/v = 1:1, 10 mL), filtered off, washed with ether, and dried over P₂O₅ to give 14-bromo-daunorubicin (4, 0.19 g, 84 %) as a red solid (m.p. 176–177 °C). 14-Bromo-daunorubicin (415.6 mg, 0.625 mmol) and 1,1',2-tris-norsqualenoic acid (320 mg, 0.80 mmol) were dissolved in acetone (150 mL) under inert Argon atmosphere. Potassium carbonate (260 mg, 1.875 mmol) was then added and the reaction mixture was stirred at room temperature for 24 h (dark). The solvent was evaporated and the crude product was purified by silica gel flash column chromatography (95:5, CH₂Cl₂–MeOH) to give a red powder (Scheme S1, 365.5 mg, 63 %). The target compound dissolved in anhydrous THF (325 mg in 22 mL) was then converted to hydrochloride salt by adding a anhydrous, titrated 1.64 M solution of HCl in dioxane (1.2 eq, 0.185 ml) and stirring at 20 °C for 2 h. The solvents were then removed and the red solid product was further purified by washing with diisopropylether. The yield of squalenoyl doxorubicin hydrochloride (SQ-Dox) was 303 mg (90 %). The purity of SQ-Dox was checked by SiO₂ TLC eluted CH₂Cl₂:MeOH:HCOOH:H₂O (88:15:2:1, R_f 0,5) and by HPLC-MS. ¹H NMR (methanol-d₄): 8.02 (d, 1H, H-3), 7.87 (d, 1H, H-1), 7.70 (t, 1H, H-2), 5.46 (s, 1H, H-10), 5.3–5.25 (m, 2H, H-14a, H-14b) and 5.20 (s, 5H, C(sq-H)), 5.19 (s, 1H, H-7), 4.15 (q, 1H, H-50), 4.01 (s, 3H, OCH₃), 3.74 (m, 2H, H-30, H-40), 3.24 (d, 1H, H-10), 3.00 (d, 1H, H-10), 2.43 (m, 1H, H-8), 2.29 and 2.35 (s 4H, CH₂ SQ acid), 2.13 (m, 1H, H-8), 2.03 (m, 16H, CH₂ SQ), 1.97 (m, 1H, H-20), 1.82 (m, 1H, H-20), 1.71 (m, 18H, C(SQ)-CH₃), 1.29 (d, 3H, CH₃); HPLC: Waters XTerra RP-18 column eluted with water, methanol, (starting 50:50, and then after 7 min

gradient up to 100 % methanol, 15 min) plus formic acid 0.05 %, elution time 28.95 min. The elution was monitored at 234 and 480 nm using a Waters 2996 Photodiode Array detector. ESI MS (Waters micromass) m/z calculated for $[C_{54}H_{71}NO_{12} + H]^+$ 927.14, found 927.2. Elemental Analysis: calculated C, 67.38; H, 7.54; Cl, 3.68; N, 1.46; found C 67.42; H, 7.61; Cl 3.67; N, 1.42.



Scheme S1. SQ-Dox synthesis

Spectroscopic characterization of Dox and SQ-Dox. Dox and SQ-Dox solutions were prepared at a concentration of 104 μM in water and loaded into a quartz cell. Absorbance profiles were obtained using a LS25 Spectrophotometer (Perkin Elmer). Fluorescence profiles were obtained using a LS-50B luminescence spectrometer (Perkin Elmer). Samples were excited at 480 nm.

Langmuir Film Balance. The compression properties of a SQ-Dox monolayer were characterized at a constant temperature of 293K using a computer-controlled KSV-Nima Langmuir-Blodgett balance coupled to

a Wilhelmy plate Device (Biolin Scientific). 100 μL of a 1 mg mL^{-1} SQ-Dox solution in $\text{CHCl}_3:\text{MeOH}$ (9:1 v:v) was spread onto pure water. After deposition, the solvents were allowed to evaporate for 10 min before compression of the monolayer at a rate of 5 $\text{\AA}^2/\text{molec}/\text{min}$. Experiments were performed at 22 $^\circ\text{C}$.

The compressibility modulus $K = C_s^{-1}$ was deduced from the obtained surface pressure-molecular area (π -A) isotherms using $K = -A \, d\pi/dA$. K is indicative of the physical state of the monolayer: liquid expanded for $13 < K < 100 \text{ mN}\cdot\text{m}^{-1}$ and liquid condensed for $100 < K < 250 \text{ mN}\cdot\text{m}^{-1}$

Packing parameter. The packing parameter was defined as $p = V/A_0 l_c$ where V and l_c were the volume and the maximum effective length of the hydrophobic chain, respectively, and A_0 the area per molecule at the amphiphilic molecule-water interface.

The stretched chain length was composed of 10 C-C-C units, with 2.5 \AA length, for a total SQ chain length l_c of 25.0 \AA (Figure S12).

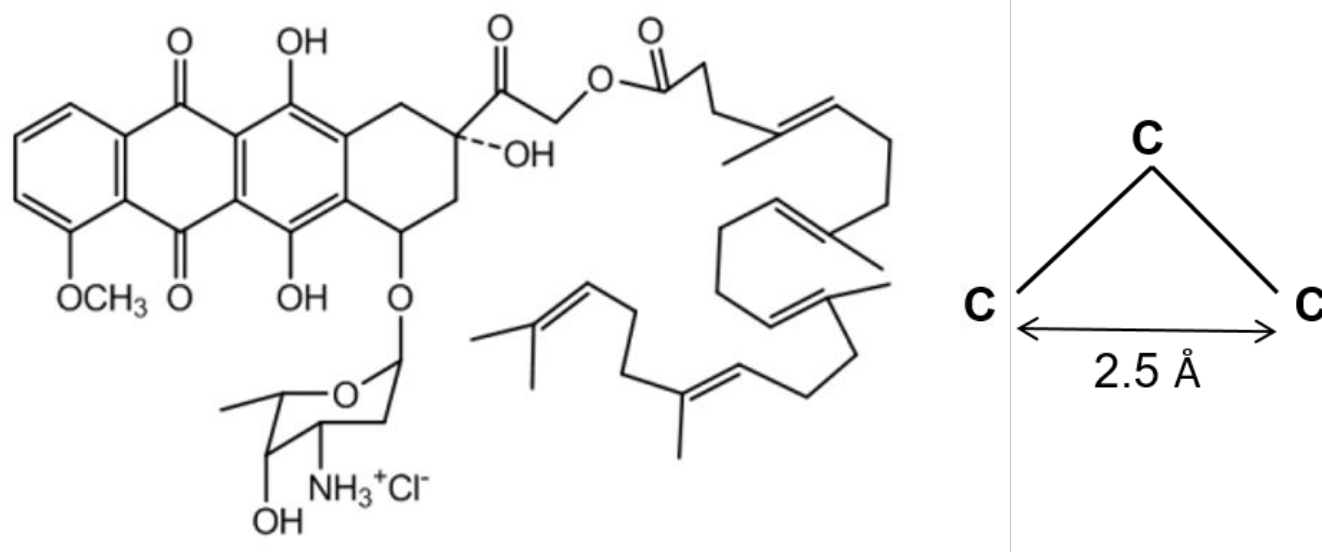


Figure S12. SQ-Dox structure.

The chain volume V was calculated as follow:

$$V = \frac{M}{\mu \cdot N_A}$$

where M was the molar mass of SQ (353 g.mol^{-1}), μ the volumic mass of SQ ($8.6 \cdot 10^{-7} \text{ g.m}^{-3}$) and N_A the Avogadro number ($6.02 \times 10^{23} \text{ mol}^{-1}$). The calculated value for V was 681 \AA^3 .

Ultracentrifugation of SQ-Dox nanoparticles. To attempt to separate the different populations, the SQ-Dox nanoparticles were centrifuged during 2 h at 40 000 g and 20 °C using an Optima CO-LE80K centrifuge equipped with a 70.1 Ti rotor (Beckman Coulter). The obtained pellet and supernatant were characterized by SAXS.

Fitting of SAXS patterns. The software package SASfit was used for the analysis of the SAXS data. The experimental SAXS patterns of SQ-Dox suspensions with or without added NaCl could be fitted using the expression that describes the scattering pattern of non-interacting core-shell cylinders (or core-shell ellipsoidal nanoparticles for 2 mM concentration in the absence of added salt). The parameters are the core radius, the shell width, the cylinder length and the scattering length densities of the core, the shell and the solvent. The scattering intensity depends on the contrast, *i.e.*, on the squared difference in the scattering length density between the core and the shell, on one hand, and the shell and the aqueous medium, on the other hand. The scattering length density is given by $\rho_L = \rho b_e$, where ρ is the electronic density of the medium and b_e is the Thomson scattering length ($b_e = 0.28179 \times 10^{-12} \text{ cm}$). Homogeneous electronic densities were assumed for the SQ core and the Dox shell. The electronic densities of SQ and water were calculated as $\rho = N_e \times N_A / V_{\text{mol}}$, where N_e is the number of electrons in one molecule, N_A the Avogadro constant and V_{mol} the molar volume of the compound (Table S2). In the absence of a known value for the molar volume of Dox, the scattering length density of the Dox shell was determined by fitting of the SAXS curves. Values in the range $\sim 1.20 \times 10^{11} - 1.35 \times 10^{11} \text{ cm}^{-2}$ were obtained for $\rho_L(\text{Dox})$, in good agreement with the electronic density of Dox headgroups in simulated SQ-Dox bilayers. Of note, bound Cl^- ions can increase the scattering length density of the Dox shell. The marked oscillation of $I(q)$ at about $q = 0.15 \text{ \AA}^{-1}$ arises from the contrast between the Dox shell and the SQ core and surrounding water.

Molecule	V_{mol} (cm ³)	N_e (e)	ρ (e/cm ³)	ρ_L (cm ⁻²)
H ₂ O	18	10	3.33 10 ²³	0.942 10 ¹¹
Squalene (C ₃₀ H ₅₀)	478	230	2.90 10 ²³	0.816 10 ¹¹

Table S2: Electronic densities and scattering lengths calculations.

The wormlike micelle models calculate the form factor for a semi-flexible cylinder with a circular cross-section and a uniform scattering length density. The fit parameters are the cylinder radius, the contour length and the Khun length of the wormlike nanoparticle. The Khun length is $2l_p$ (l_p is the persistence length). The overall contour length, being outside the resolution of the SAXS experiment (~ 100 nm), was fixed to 1000 nm.

Calculation of Debye lengths. The Debye lengths λ_D for SQ-Dox nanoparticles were calculated using $\lambda_D = (\epsilon_0 \epsilon_r k_B T / 2e^2 I)^{1/2}$ where ϵ_0 is the vacuum permittivity, ϵ_r the dielectric constant of water, k_B the Boltzmann constant, T the absolute temperature, e the elementary charge and I the ionic strength. In the absence of added salt, the ionic strength was determined assuming a total dissociation of the Cl⁻ counter ions. When NaCl was added to SQ-Dox nanoparticles, it was calculated by adding the salt contribution to the ionic strength of the counterions.

Molecular Dynamics

Analysis of SQ-Dox aggregates. For the sake of analysis the SQ-Dox molecule was divided into three structural parts: the “tail” (*i.e.*, the squalene moiety including the linker), the “rings” (the tetracene part of Dox) and the sugar. The distances between the groups were measured as the distances between their centers of masses.

The orientation of the rings was determined by the long and short axes and the normal to tetracene rings, which is a cross product of the former (Figure S6d).

The rings formed stacked aggregates in the course of the simulation and were classified depending on the relative orientations of their long and normal axes. The aggregates were encoded as n-n where the first letter showed whether long axes of two molecules were parallel (“p”) or antiparallel (“a”) and the second letter showed the same for normal axis. Thus “p-p” means that both axes are parallel, “a-a” means that both of them are antiparallel, *etc.* All four possible types of aggregates are shown in Figure 2. Noteworthy, “p-p” stacking in the context of this work only means parallel orientation of involved molecules and should not be mistaken with π - π stacking of π orbitals in general chemical meaning.

Potentials of mean force for stacking interaction. In order to estimate the strength of the stacking interaction between the rings of two SQ-Dox molecules the lone stacked pair was selected in equilibrated cylindrical nanoparticle by visual inspection. The distance between the rings was restrained by harmonic potential with the force constant of $2000 \text{ kJ.mol}^{-1}.\text{nm}^{-2}$ at equally spaced points from 0.3 nm to 1.0 nm, which resulted in 15 umbrella sampling windows. Each window was simulated for 40 ns and the last 10 ns were used for analysis. The potential of mean force (PMF) was obtained with the weighted histogram technique³ as implemented in Gromacs package.

Interaction of cylindrical nanoparticles. In order to study the interaction between cylindrical nanoparticles, two pre-equilibrated nanoparticles were arranged parallel to each other. The weak flat-bottom potential with the force constant of $200 \text{ kJ.mol}^{-1}.\text{nm}^{-2}$ was applied between their centers of masses in XY plain to restrict their diffusion beyond the distance of 5 nm and to keep their surfaces in contact. The system was simulated for 300 ns.

Pre-arranged three-layer bilayer tubes. Three-layer tubes were constructed to mimic the experimentally observed structures. The central part of the tube was modelled by the pre-equilibrated cylindrical micelle. The outer bilayer tube was constructed independently from SQDox molecules arranged into two concentric cylindrical shells with Dox moieties facing internal lumen and outer solvent respectively. Inner and outer

leaflets contained 180 and 300 SQ-Dox molecules respectively. The tube was infinite in Z direction due to periodic boundary conditions. The system was initially solvated with ~32000 water molecules, 446 SO_4^{2-} ions and Na^+ counter ions to achieve electro neutrality. The system was pre-equilibrated in a series of four short simulations (10 ps each). At the end of each such simulation compactization of the bilayer creates a free volume inside the tube, which is isolated from the outer water bath and thus cannot be filled by water molecules. This volume was solvated manually in an iterative manner. After reaching equilibrium water density inside the tube, the inner cylindrical micelle was inserted manually into the lumen. Overlapping water molecules and ions were removed and the system was energy minimized to relax any remaining steric clashes. After that the system was equilibrated for 100 ns. Last 30 ns were used for analysis.

Technical details. All simulations were performed in Gromacs package versions 5.1.2, 2016.1 and 2018.1.⁴ TIP3P water model was used. All simulations were performed in NPT conditions with temperature of 320 K and pressure of 1 bar maintained by v-rescale thermostat and Parrinello-Rahman barostat respectively. The time step of 2 fs was used with all bonds converted to rigid constraints. An integration step of 2 fs was used. Long range electrostatics was computed with the PME method.⁵ This choice of the parameters was used with great success in our previous work.^{6,7} Preparation of the systems and data analysis was performed with Pteros 2.0 molecular modeling library.^{8,9} VMD 1.9.2 was used for visualization.¹⁰

IV. REFERENCES

- (1) Changenet-Barret, P.; Gustavsson, T.; Markovitsi, D.; Manet, I.; Monti, S. Unravelling Molecular Mechanisms in the Fluorescence Spectra of Doxorubicin in Aqueous Solution by Femtosecond Fluorescence Spectroscopy. *Phys. Chem. Chem. Phys.* **2013**, *15*, 2937-2944.
- (2) Maksimenko, A.; Dosio, F.; Mougin, J.; Ferrero, A.; Wack, S.; Reddy, L. H.; Weyn, A.-A.; Lepeltier, E.; Bourgaux, C.; Stella, B.; Cattel, L.; Couvreur, P. A Unique Squalenoylated and Nonpegylated Doxorubicin Nanomedicine with Systemic Long-Circulating Properties and Anticancer Activity. *Proc. Natl. Acad. Sci. U. S. A.* **2014**, *11*, E217–E226.
- (3) Kumar, S.; Rosenberg, J. M.; Bouzida, D.; Swendsen, R. H.; Kollman, P. A. The Weighted Histogram Analysis Method for Free-Energy Calculations on Biomolecules. I. The Method. *J. Comput. Chem.* **1992**, *13*, 1011–1021.
- (4) Abraham, M. J.; Murtola, T.; Schulz, R.; Páll, S.; Smith, J. C.; Hess, B.; Lindahl, E. GROMACS: High Performance Molecular Simulations through Multi-Level Parallelism from Laptops to Supercomputers. *SoftwareX* **2015**, *1-2*, 19–25.
- (5) Van Der Spoel, D.; Lindahl, E.; Hess, B.; Groenhof, G.; Mark, A. E.; Berendsen, H. J. C. GROMACS: Fast, Flexible, and Free. *J. Comput. Chem.* **2005**, *26*, 1701–1718.
- (6) Yesylevskyy, S. O.; Rivel, T.; Ramseyer, C. The Influence of Curvature on the Properties of the Plasma Membrane. Insights from Atomistic Molecular Dynamics Simulations. *Sci. Rep.* **2017**, *7*, 16078.
- (7) Sobot, D.; Mura, S.; Yesylevskyy, S. O.; Dalbin, L.; Cayre, F.; Bort, G.; Mougin, J.; Desmaële, D.; Lepetre-Mouelhi, S.; Pieters, G.; Andreiuk, B.; Klymchenko, A. S.; Paul, J.-L.; Ramseyer, C.; Couvreur, P. Conjugation of Squalene to Gemcitabine as Unique Approach Exploiting Endogenous Lipoproteins for Drug Delivery. *Nat. Commun.* **2017**, *8*, 15678.

- (8) Yesylevskyy, S. O. Pteros: Fast and Easy to Use Open-Source C++ Library for Molecular Analysis. *J. Comput. Chem.* **2012**, *33*, 1632–1636.
- (9) Yesylevskyy, S. O. Pteros 2.0: Evolution of the Fast Parallel Molecular Analysis Library for C++ and Python. *J. Comput. Chem.* **2015**, *36*, 1480–1488.
- (10) Humphrey, W.; Dalke, A.; Schulten, K. VMD: Visual Molecular Dynamics. *J. Mol. Graph.* **1996**, *14*, 33–38.